Published in final edited form as:
Nat Photonics. 2008 ; 2(2): 86–89. doi:10.1038/nphoton.2007.277.

Dynamic manipulation and separation of individual semiconducting and metallic nanowires

Arash Jamshidi[1,†], **Peter J. Pauzauskie**[2,3,†,~], **P. James Schuck**[4], **Aaron T. Ohta**[1], **Pei-Yu Chiou**[5], **Jeffrey Chou**[1], **Peidong Yang**[2,3,*], and **Ming C. Wu**[1,*]

[1]Department of Electrical Engineering, University of California, Berkeley, CA 94720, USA

[2]Department of Chemistry, University of California, Berkeley, CA 94720, USA

[3]Materials Science Division, Lawrence Berkeley National Laboratory, Berkeley, CA 94720, USA

[4]Molecular Foundry, Lawrence Berkeley National Laboratory, Berkeley, CA 94720, USA

[5]Department of Mechanical and Aerospace Engineering, University of California, Los Angeles (UCLA), Los Angeles, CA 90095, USA

Abstract

The synthesis of nanowires has advanced in the last decade to a point where a vast range of insulating, semiconducting, and metallic materials[1] are available for use in integrated, heterogeneous optoelectronic devices at nanometer scales [2]. However, a persistent challenge has been the development of a general strategy for the manipulation of individual nanowires with arbitrary composition. Here we report that individual semiconducting and metallic nanowires with diameters below 20 nm, are addressable with forces generated by optoelectronic tweezers (OET) [3]. Using 100,000× less optical power density than optical tweezers, OET is capable of transporting individual nanowires with speeds 4× larger than maximum speeds achieved by optical tweezers. A real-time array of silver nanowires is formed using photopatterned virtual-electrodes, demonstrating the potential for massively parallel assemblies. Furthermore, OET enables the separation of semiconducting and metallic nanowires, suggesting a broad range of applications for the separation and heterogenous integration of one-dimensional nanoscale materials.

One approach for the organization of materials with nanometer-scale dimensions [4] is the so-called 'bottom-up' assembly of heterogeneous building blocks [5]. Though it is possible to achieve a high level of orientation control [6, 7] through epitaxial growth of semiconductor materials [8], there are enormous challenges to achieving a high level of integration with heterogeneous material systems due to large differences in chemical and thermal stability. One way to circumvent the constraints of thermo-chemical incompatibility is first to synthesize various materials at favorable processing conditions, then employ a strategy for post-synthesis integration.

Several techniques have been employed over the last decade to enable nanowire integration. Advances in microcontact printing have opened up the possibility to coat macroscopically-large areas with inorganic nanowires or carbon nanotubes [9]. Microfluidic [10, 11] and Langmuir-Blodgett [12-14] patterning also have been used to align large numbers of nanowires dispersed

*To whom correspondence should be addressed, P.Y. (p_yang@berkeley.edu) or M.C. W. (wu@eecs.berkeley.edu)..
~Present Address: Chemistry, Materials, and Life Sciences Directorate, Lawrence Livermore National Laboratory, 7000 East Ave., L-235, Livermore, CA 94551
†These authors contributed equally to this work.

Competing financial interests: The authors declare no competing financial interests.

in a fluid matrix. The manipulation of single structures requires more precise control, which has been achieved using motorized nanomanipulators [15] or optical traps [16]. Dielectrophoresis (DEP) [17-19] is another approach that has been employed recently to manipulate suspended 1D-nanostructures. In this technique, microfabricated electrodes are used to produce an AC potential that polarizes the given 1D-nanostructure, forcing it to align with the electric field lines between the patterned electrodes. The non-uniform electric field present in the liquid layer induces a dipole in the nanostructures and attracts them to the region of highest field gradient. The DEP force expression for a spherical particle is given [20] by $F_{DEP} = 2\pi r^3 \varepsilon_m \mathrm{Re}\{K\} \nabla E^2$ where r is the radius of the particle, ε_m is the permittivity of the media, Re{*K*} is the real part of the Clausius-Mossotti (C.M.) factor (*K*), and ∇E^2 is the gradient of the squared electric field. The C.M. factor is a function of the permittivity and conductivity of the particle and the media, and in the case of spherical particles, has a value between −0.5 and 1. Although the approach has yielded impressive nanostructure alignment [18] and separations [17], it is constrained as the DEP electrodes are fixed in place, and are unable to arrange individual nanostructures into real-time reconfigurable patterns.

Optoelectronic tweezers (OET) have emerged as a powerful tool for massively parallel manipulation of polymer-beads and living cells at micron length-scales via optically-induced dielectrophoresis [3]. Two-dimensional patterns of low-intensity light are projected onto a plane of photoconductive material sandwiched between transparent parallel-plate electrodes. The light excites carriers in the photoconductive layer (hydrogenated amorphous silicon), reducing the local impedance to create an inhomogeneous electric field across the liquid layer. In the presence of the non-uniform electric field, a polarization is induced in particles between the parallel plates. The polarized particles are either attracted to or repelled from the field gradient (as in DEP) produced by the projected light pattern, yielding a powerful optoelectronic method of particle manipulation based on dynamic, light-actuated virtual electrodes[21].

Although this approach works extremely well for micron-scale objects, the forces generated with OET typically are overcome by thermal (Brownian) fluctuations when particles are much smaller than 1 μm, as DEP force scales with r^3. The theory of dielectrophoretic trapping [20] suggests that one way to manipulate objects with sub-micron dimensions is to work with highly elongated structures, where two dimensions of the particle can be significantly below 100 nm, while the third dimension is on the order of micrometers. Modeling the force using an elongated ellipsoid model [20], the DEP force for a nanowire is given by $F_{DEP} = (\pi r^2 l/6)\varepsilon_m \mathrm{Re}\{K\} \nabla E^2$, where *r* and *l* are the nanowire's radius and length, respectively. For nanowires that are much more polarizable than the surrounding media and have high aspect ratios, the C.M. factor can be much larger than 1.

To determine whether OET forces could address nanowires suspended in a fluid matrix, we transferred an aqueous suspension of silicon nanowires to a device chamber illustrated in Fig. 1a. In addition, finite element simulations were employed to calculate approximate field gradients and the corresponding forces on suspended nanowires. In comparing the DEP force of a nanowire (length = 5 μm) and a spherical particle over a range of radii (Fig. 1b), it is evident that the nanowire experiences a DEP force 2-3 orders of magnitude larger than the spherical particle due to one of the dimensions of the nanowire (length) being larger than the spherical particle and the increase in the C.M. factor of the nanowire. The inset of Fig. 1b shows the simulated values of the C.M. factor for a nanowire of length 5 μm and radius 50 nm for different values of nanowire resistivity over a range of frequencies. As mentioned above, the smallest spherical particle trappable using OET is approximately 1 μm. The increase in the DEP force for the nanowire, however, makes it possible to trap individual nanowires having diameters as small as 20 nm with OET. Nanowires experience a torque in addition to the DEP force, which aligns the long-axis of the nanowire with the electric field perpendicular to the imaging plane of the OET device (Fig. 1a,d). Therefore, the nanowire is aligned vertically

within the sample chamber. Figs. 1c-e show the process of trapping an individual silicon nanowire using a 633 nm HeNe laser (10 μm FWHM and 100 W/cm^2). In Fig. 1c there is no voltage applied across the device and the nanowire undergoes Brownian motion (Supplementary Information, Video 1). Once the voltage is applied (Fig. 1d), the long axis of the nanowire aligns with the electric field in a fraction of a second and the nanowire follows the laser trap as the beam is manually scanned across the stage (Fig. 1e). Maximum trapping speeds for an individual silicon nanowire with 100 nm diameter and 5 μm length approach 135 μm/s with a peak-to-peak trapping voltage of 20V. This is approximately 4 times the maximum speed achievable by optical tweezers [16] and is reached with 5-6 orders of magnitude less optical power density than optical tweezers. In addition, OET trap stiffness figure-of-merit[22] is measured to be 1.6×10^{-6} N/(m×mW) which is approximately 2 orders of magnitude larger than typical stiffness figure-of-merit numbers reported for optical tweezers[16] (Supplementary Information, Fig. S6). Fundamentally, the size of the trapping potentials are diffraction-limited and the positioning accuracy of the wire inside the trap is limited by Brownian motion. We used particle tracking image analysis software to measure the nanowire localization to be less than 0.22 μm^2 (Supplementary Information, Fig. S3). Although a single wire is trapped in this potential well, it is possible to trap arbitrarily large numbers of wires in a given area, simply by focal adjustment of the optical spot's size (Supplementary Information, Video 2).

We have also found it is possible to preserve the position and orientation of the wires trapped with OET using a photocurable polymer[23, 24] solution such as PEGDA[25, 26], enabling immobilization of nanowires in the polymer matrix within seconds by exposing the manipulation area to an ultra-violet source. (Supplementary Information, Fig. S7, Video 3). The ability to preserve the position and orientation of OET-trapped nanowires is critical for enabling later post-processing steps, such as the deposition of metallic contacts. The polymer solution's increased viscosity and conductivity are found to reduce the speed of nanowire translation by more than a factor of 2, and future work will focus on finding optimal polymer solutions to minimize interference from viscous drag and the screening of nanowire polarizablity.

In addition to trapping semiconductor nanowires, we also demonstrated that OET is capable of trapping and manipulating metallic (silver) nanowires. Prior experiments with a single-beam infrared laser trap showed that high laser powers led to intense heating and scattering forces that prevented the optical trapping of silver nanowires [16]. Silver nanowires were found to show interesting OET trapping characteristics (Fig. 2) due to their very high polarizability which forces them to align strongly with the electric field present in the liquid layer. Fig. 2b,c show the process of trapping three silver nanowires over a period of 4s. It is interesting to note that the silver nanowires are trapped in the laser spot at an angle, as depicted in Fig. 2a. The trapping angle, θ_m, of silver wires in the OET potential (Fig. 2c) is measured to be approximately 74° using the relation $\theta_m = cos^{-1}(L_t/L_o)$, where L_o equals the total length of the horizontal, non-trapped nanowire and L_t equals the observed length of the nanowires once they are in the trap. The silver nanowires are trapped in the region of highest electric field gradient and it is expected that they align to the electric field in that region due to their high polarizability. Using the simulated values for ∇E^2 (Fig. 2a), we also calculate, θ_c, the angle of the electric field in high-∇E^2 region and find it to be approximately 64°, which is within 15% of the experimentally measured value.

As mentioned before, the strength of the DEP force depends on the relative permittivities and conductivities of the nanowire and suspension medium. Therefore, in the case of semiconducting (silicon) nanowires versus metallic (silver) nanowires, it is expected that the silver nanowires experience larger DEP force due to their higher polarizabilities. Fig. 3a shows the maximum trapping speeds achieved for individual silicon and silver nanowires for a range of peak-to-peak AC voltages. With an 8 V peak-to-peak AC bias applied across the OET device,

the silver nanowires experience speeds up to 125 μm/s while remaining trapped, whereas silicon nanowires remain trapped only for speeds ≤ 2 μm/s. Thus, it is possible to separate silicon and silver nanowires by adjusting the scanning speed of the trapping laser while using a suitable peak-to-peak AC bias; so that the silver nanowires will be captured by the laser trap while silicon nanowires will be left behind. Figs. 3b-d show the process of separating an individual silver nanowire from a silicon nanowire. The silver nanowire is aligned with the electric field even at 8 V peak-to-peak due to its high polarizablitliy, whereas the silicon nanowire is not aligned. A line laser is used to trap the silicon and silver nanowires (Fig. 3b) and as the laser is scanned across the stage, the silicon nanowire is left behind (Supplementary Information, Video 4) whereas the silver nanowire stays with the trap (Fig. 3d). In addition, control experiments were performed using silicon nanowires of comparable or larger lengths than the silver nanowires and the same separation effect was observed. We expect this approach to nanowire separations may also be extended to the separation of semiconducting and metallic carbon nanotubes. Despite the smaller cross sectional area of carbon nanotubes and the r^2 dependence of F_{DEP}, the increased aspect ratio and higher electrical conductivity of carbon nanotubes suggest OET as a promising direction for nanotube separations.

Recently there has been interest in vertically aligned nanowire arrays for solar energy conversion[27], thermoelectric cooling[28], and vertical field effect transistor[29] applications. One powerful aspect of OET is its ability to perform large-scale assembly of objects with a digital micromirror device (DMD) [3]. Figs. 4a-b show examples of large-scale assembly of nanowires using real-time dynamic trapping. Fig. 4a. shows the formation of a 5×5 array of single silver nanowires which are individually addressable in real-time (Supporting information, Fig. S2, Video 5). Another approach to formation of large-scale arrays of nanowires is to use larger trapping patterns. Fig. 4b shows the process of tuning the density of silver nanowires trapped by varying the size of a rectangular trapping pattern in real-time (Supporting information, Video 6). It is interesting to note that when multiple wires are trapped in a single potential, they are observed to repel each other and fill the active trapping pattern due to dipole-dipole interactions.

At present, many challenges remain before this approach becomes viable for large-scale nanowire integration. Manipulation is restricted to the 2D surface coated by a photoconductive thin film, limiting the construction of 3D heterostructures. Additionally, wires are observed to adhere to the samples surface through non-specific binding which limits the ease of manipulation. However, it has been demonstrated recently that nanowire surface functionalization is an effective tool to control interactions between nanowires and surfaces[30] and these methods can potentially be used to reduce the nanowire adhesion. One promising future direction involves trapping nanowires in lateral directions and immobilization of the nanowires for construction of three-dimensional heterostructures from metallic and semiconducting nanowires [31]. However, in its present form, real-time OET offers parallel, high-speed manipulation for a broad range of one-dimensional materials, enabling dynamic positioning and rapid separation of semiconducting and metallic nanowires. In principle, the technique may be extended to microfluidic chambers and applied to the separation of other materials, such as carbon nanotubes [17, 32] or to the construction of thermoelectric arrays [28].

Methods

Optoelectronic Tweezers

The OET device consists of a top indium-tin oxide (ITO) transparent electrode, and a bottom ITO electrode coated with a 1-μm layer of hydrogenated amorphous silicon (a-Si:H). Fig. 1a shows the device structure of the optoelectronics tweezers (OET). The liquid layer containing the nanowire sample is sandwiched between the top and the bottom layers. There is an AC voltage bias applied between the top and the bottom electrode. To actuate the a-Si:H layer, a

633 nm HeNe laser is used. When there is no laser present, the voltage is dropped across the aSi:H layer. However, once the laser is turned on, it generates electron-hole pairs in the a-Si:H layer and the voltage is transferred to the liquid layer where the laser is present. The voltage in the liquid layer above the illuminated area creates a non-uniform electric field pattern across the liquid layer.

Dynamic Trap Generation

By programming a digital micromirror spatial light modulator (Texas Instruments, 1,024×768 pixels, 13.68 μm × 13.68 μm pixel size), it is possible to create real-time, dynamic, flexible trapping patterns for trapping and separating the individual nanowires. A 635 nm semiconductor laser is expanded, covering the spatial light modulator area. The spatial light modulator images are controlled through a GUI interface, which is capable of creating arbitrarily configured real-time traps by focusing the images onto the OET chip surface using a 10× objective. (Supplementary Information, Videos 5, 6, and 7).

Finite-Element Analysis

Simulations of the electric field gradient produced at virtual electrodes in the optoelectronic tweezers were performed with commercial software (COMSOL Multiphysics).

Particle Tracking Analysis

Nanowire tracking analysis were done using the IDL-based particle tracking software developed by J. Crocker and E. R. Weeks.

Synthesis

Silicon nanowires in Figs. 3, S2, and S3 were grown by chemical vapor deposition (CVD) of silicon tetrachloride ($SiCl_4$) onto a silicon wafer, which was gold coated by e-beam evaporation of Au, in a 850°C furnace for approximately 30 minutes [33]. Silicon nanowires used in Figs. 1› S4, and S5 were etched from single-crystal silicon wafers following electroless metal deposition [34]. Silver nanowires were prepared using poly(vinyl pyrrolidone) (PVP) as the capping agent [35] and were found to have diameters of 80 to 100 nm, and lengths from 1 to 10 μm.

Supplementary Material

Refer to Web version on PubMed Central for supplementary material.

Acknowledgements

This work was supported in part by the National Institutes of Health (NIH) through the NIH Roadmap for Medical Research (Grant #PN2 EY018228), Defense Advanced Research Project Agency (DARPA) UPR-CONSRT, the Institute for Cell Mimetic Space Exploration (CMISE), Dreyfus Foundation, and the U.S. Department of Energy (PY). PJP and ATO thank the National Science Foundation (NSF) for a graduate research fellowship. Work at the Lawrence Berkeley National Laboratory was supported by the Office of Science, Basic Energy Sciences, Division of Materials Science of the U.S. Department of Energy, with The Molecular Foundry portion supported under Contract No. DE-AC02-05CH11231. We thank the National Center for Electron Microscopy for the use of their facilities, Ali Javey, Roie Yerushalmi, Hsan-Yin Hsu, Steven Neale, Eudean Sun, and Justin Valley for helpful discussions and suggestions, and also Jiaxing Huang, Raül Diaz, and Erik Garnett for silver and silicon nanowire samples.

References

1. Xia YN, et al. One-dimensional nanostructures: synthesis, characterization, and applications. Adv. Mater 2003;15:353–389.
2. Pauzauskie PJ, Yang P. Nanowire photonics. Materials Today 2006;9:36–45.

3. Chiou PY, Ohta AT, Wu MC. Massively parallel manipulation of single cells and microparticles using optical images. Nature 2005;436:370–372. [PubMed: 16034413]
4. Sirbuly DJ, Law M, Yan HQ, Yang PD. Semiconductor nanowires for subwavelength photonics integration. J. Phys. Chem. B 2005;109:15190–15213. [PubMed: 16852925]
5. Law M, et al. Nanoribbon waveguides for subwavelength photonics integration. Science 2004;305:1269–1273. [PubMed: 15333835]
6. Pauzauskie PJ, et al. Crystallographic alignment of high-density gallium nitride nanowire arrays. Nat. Mater 2004;3:524–528. [PubMed: 15273744]
7. He R, Yang P. Giant piezoresistance effect in silicon nanowires. Nat Nanotechnol 2006;1:42–46. [PubMed: 18654140]
8. Martensson T, et al. Epitaxial III-V nanowires on silicon. Nano Lett 2004;4:1987–1990.
9. Ahn JH, et al. Heterogeneous three-dimensional electronics by use of printed semiconductor nanomaterials. Science 2006;314:1754–1757. [PubMed: 17170298]
10. Huang Y, Duan XF, Wei QQ, Lieber CM. Directed assembly of one-dimensional nanostructures into functional networks. Science 2001;291:630–633. [PubMed: 11158671]
11. Messer B, Song JH, Yang PD. Microchannel networks for nanowire patterning. J. Am. Chem. Soc 2000;122:10232–10233.
12. Yang P. Nanotechnology: Wires on water. Nature 2003;425:243–244. [PubMed: 13679895]
13. Tao A, et al. Langmuir-Blodgett silver nanowire monolayers for molecular sensing using surface-enhanced Raman spectroscopy. Nano Lett 2003;3:1229–1233.
14. Jin S, et al. Scalable interconnection and integration of nanowire devices without registration. Nano Lett 2004;4:915–919.
15. Sirbuly DJ, et al. Optical routing and sensing with nanowire assemblies. Proc. Natl. Acad. Sci. U S A 2005;102:7800–7805. [PubMed: 15911765]
16. Pauzauskie PJ, et al. Optical trapping and integration of semiconductor nanowire assemblies in water. Nat. Mater 2006;5:97–101. [PubMed: 16429143]
17. Krupke R, Hennrich F, von Lohneysen H, Kappes MM. Separation of metallic from semiconducting single-walled carbon nanotubes. Science 2003;301:344–347. [PubMed: 12829788]
18. Smith PA, et al. Electric-field assisted assembly and alignment of metallic nanowires. Appl. Phys. Lett 2000;77:1399–1401.
19. Lee SY, et al. An electrical characterization of a hetero-junction nanowire (NW) PN diode (n-GaN NW/p-Si) formed by dielectrophoresis alignment. Physica E 2007;36:194–198.
20. Jones, TB. Electromechanics of particles. Cambridge University Press; 1995.
21. Ohta AT, et al. Dynamic cell and microparticle control via optoelectronic tweezers. J. Micromech. S 2007;16:491–499.
22. Neale SL, Mazilu M, Wilson JIB, Dholakia K, Krauss TF. The resolution of optical traps created by light induced dielectrophoresis (LIDEP). Opt. Express 2007;15:12619–12626. [PubMed: 19550529]
23. Decker C. Kinetic study and new applications of UV radiation curing. Macromol. Rapid Commun 2002;23:1067–1093.
24. Beebe DJ, et al. Functional hydrogel structures for autonomous flow control inside microuidic channels. Nature 2000;404:588–590. [PubMed: 10766238]
25. Albrecht DR, Tsang VL, Saha RL, Bhatia SN. Photo- and electropatterning of hydrogel-encapsulated living cell arrays. Lab Chip 2005;5:111–118. [PubMed: 15616749]
26. Liu VA, Bhatia SN. Three-dimensional photopatterning of hydrogels containing living cells. Biomed. Microdevices 2002;4:257–266.
27. Law M, Greene L, Johnson JC, Saykally R, Yang P. Nanowire dye-sensitized solar cells. Nat. Mater 2005;4:455–459. [PubMed: 15895100]
28. Dresselhaus MS, et al. New directions for low-dimensional thermoelectric materials. Adv. Mater 2007;19:1043–1053.
29. Goldberger J, Hochbaum AI, Fan R, Yang P. Silicon vertically integrated nanowire field effect transistors. Nano Lett 2006;6:973–977.

30. Yerushalmi R, Ho JC, Jacobson ZA, Javey A. Generic nanomaterial positioning by carrier and stationary phase design. Nano Lett 2007;7:2764–2768. [PubMed: 17661524]

31. Ohta AT, et al. Optically controlled cell discrimination and trapping using optoelectronic tweezers. IEEE J. Sel. Top. Quant 2007;13:235–243.

32. Arnold MS, Green AA, Hulvat JF, Stupp SI, Hersam MC. Sorting carbon nanotubes by electronic structure using density differentiation. Nat. Nanotechnol 2006;1:60–65. [PubMed: 18654143]

33. Hochbaum AI, Fan R, He R, Yang P. Controlled growth of Si nanowire arrays for device integration. Nano Lett 2005;5:457–460. [PubMed: 15755094]

34. Peng KQ, Yan YJ, Gao SP, Zhu J. Synthesis of large-area silicon nanowire arrays via self-assembling nanoelectrochemistry. Adv. Mater 2002;14:1164–1167.

35. Sun YG, Gates B, Mayers B, Xia YN. Crystalline silver nanowires by soft solution processing. Nano Lett 2002;2:165–168.

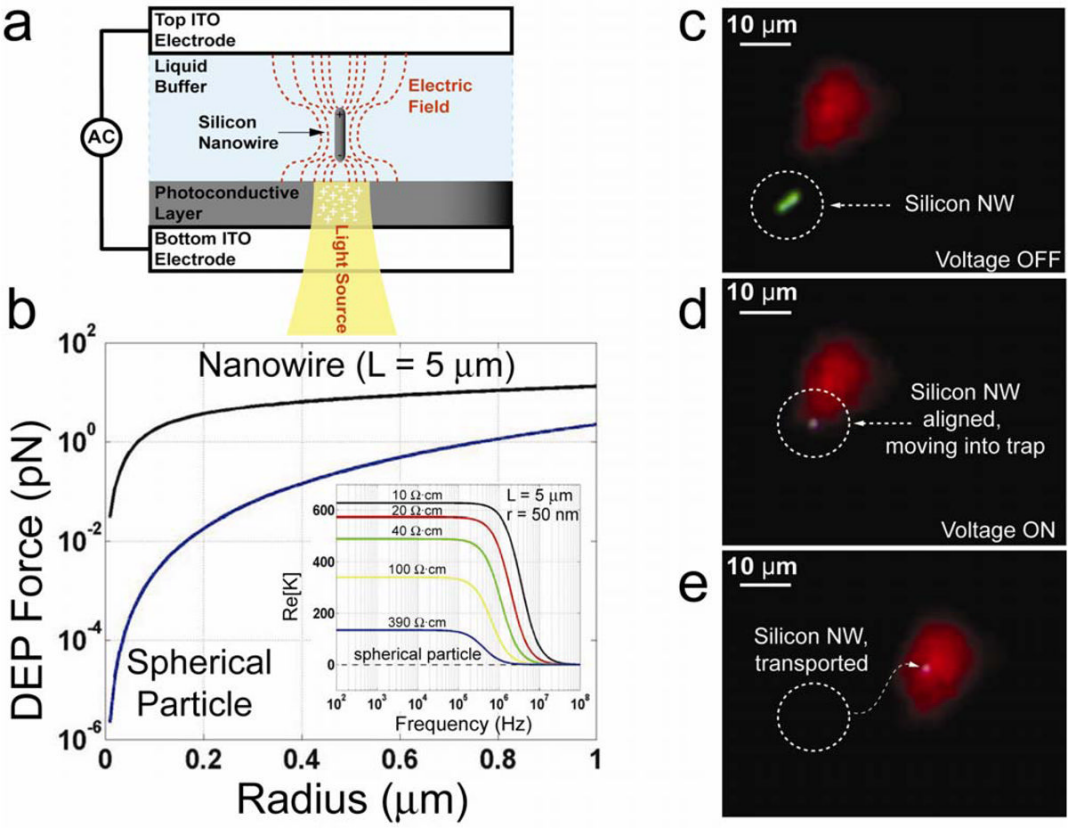

Figure 1. OET manipulation of single silicon nanowire

a, Optoelectronic tweezers device structure with an individual nanowire trapped at the laser spot. **b**, Comparison of the DEP force for a 5-μm-long nanowire and a spherical particle as a function of radius. The inset shows the simulated values of the Clausius-Mossotti factor over a range of frequencies for different nanowire conductivities (for a nanowire with a 5 μm length, and a 50 nm diameter). **c – e**, Trapping of an individual silicon nanowire using a laser spot; **c**, No voltage is applied across the device, and the nanowire undergoes Brownian motion; **d**, The voltage is applied, the long-axis of the nanowire aligns with the electric field and the nanowire moves into the trap; **e**, The nanowire follows the laser trap position.

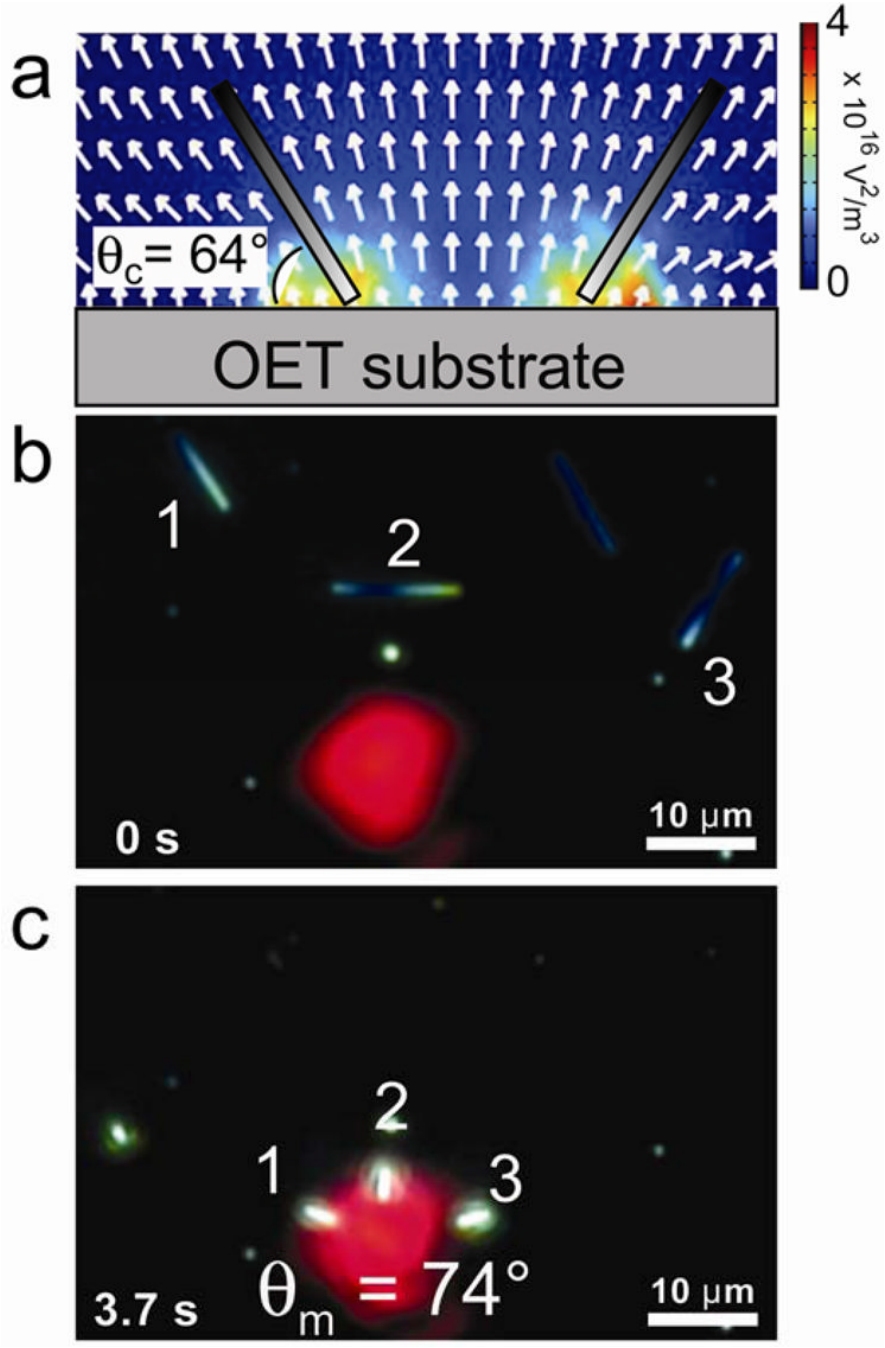

Figure 2. OET manipulation of silver nanowires

a, Simulation of ∇E^2 (color plot) and the electric field (arrows) for a 50 kHz, 8V peak-to-peak bias applied to the device. The electric field in the area of highest ∇E^2 (where the wires are trapped) is calculated to have an angle of $\theta_c = 64°$ with the OET surface. **b**, No voltage is applied to the device, therefore the silver nanowires undergo Brownian motion and are not attracted to the laser spot. **c**, Once the voltage is turned on the nanowires align with the electric field and are trapped in the laser spot at an angle of approximately $\theta_m = 74°$ which is within 15% of the calculated value.

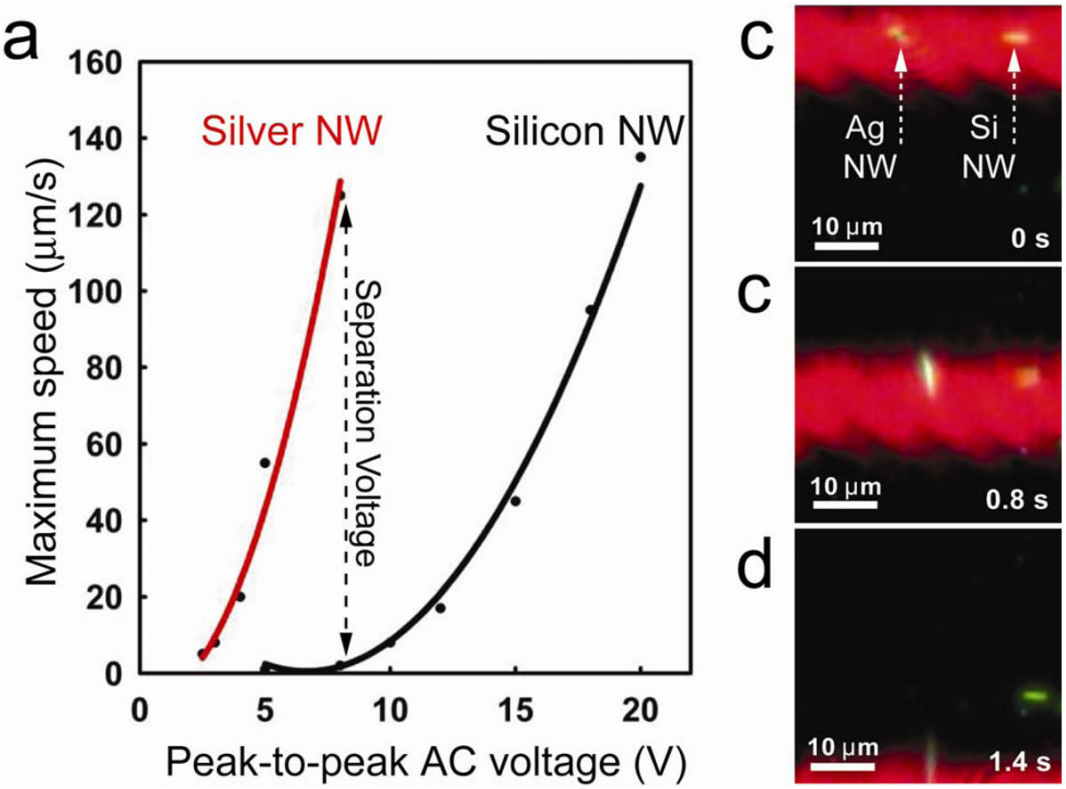

Figure 3. Dynamic separation of semiconducting and metallic nanowires

Separation process of an individual silver nanowire from an individual silicon nanowire by adjusting the scanning speed of a line laser. **a**, Maximum experimental trapping speed for an individual silicon and silver nanowire over a range of peak-to-peak AC voltages. Due to the high polarizability of silver nanowires, at 8 V peak-to-peak, the silver nanowires experience speeds up to 125 μm/s while silicon nanowires only experience speeds less than 2 μm/s. The solid lines in the plot are quadratic fits to the experimental data points. **b**, Both silver and silicon nanowires rest in the stationary trapping potential. **c**, The translation of the line potential begins the separation. **d**, Scanning of the laser line with speeds greater than approximately 2 μm/s causes final separation of the silver and silicon nanowires.

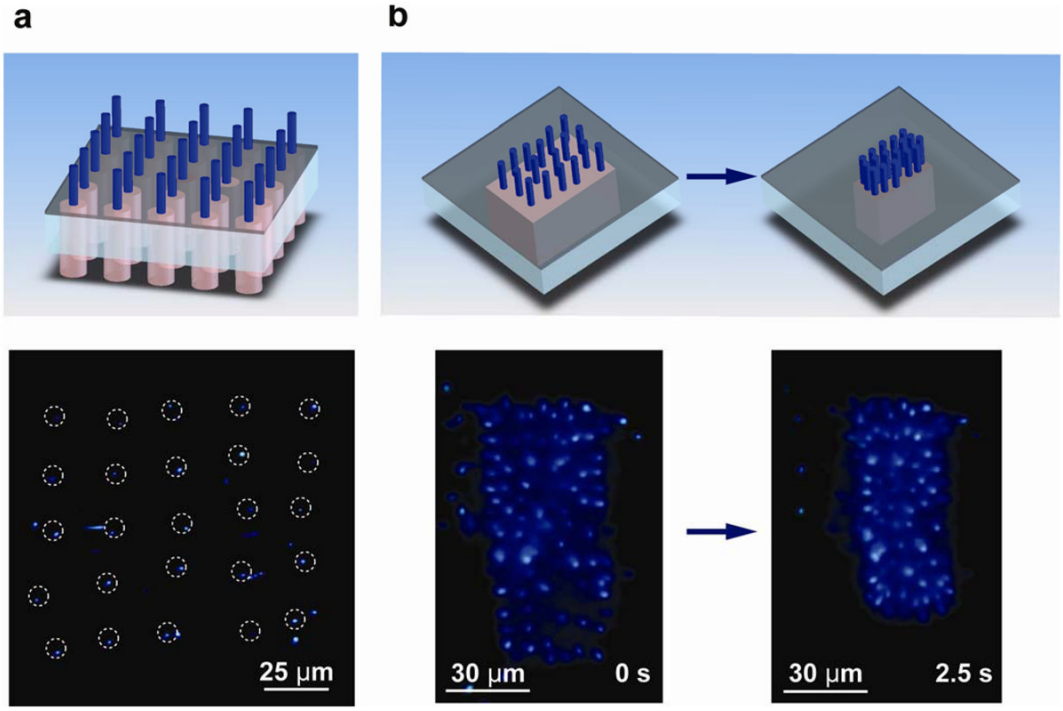

Figure 4. Large-scale assembly of nanowires

Large-scale manipulation of silver nanowires using traps created with a digital micromirror spatial light modulator and positioned with a computer-mouse-controlled GUI. **a**, Formation of a 5×5 single silver nanowire array **b**, Large-scale control of nanowire density by adjusting the size of the trapping pattern. A collection of more than 80 silver nanowires is concentrated from an area of approximately 3000 $(\mu m)^2$ to 2000 $(\mu m)^2$. The laser source is filtered out digitally in the images to aid pattern observation.